Imaging of stratified media using high-speed swept source optical coherence tomography

Maddipatla Reddikumar[1] and Raju Poddar[1,2,*]

[1]Applied Optics Laboratory, Department of Applied Physics, and
[2]Department of Bio-Engineering, Birla Institute of Technology-Mesra, Ranchi 835 215, India

We demonstrate a noninvasive, three-dimensional, depth-resolved imaging of stratified media with a swept source optical coherence tomography (SS-OCT) system at 1064 nm centre wavelength. A swept source laser is used to enable imaging rate of 100 kHz (100,000 A-scans/s). A comparison between SS-OCT and other imaging modalities is also presented. Brief theory, detail instrumentation of the system and signal processing method are described. The system has axial and transverse resolution of 5 and 14 μm in air respectively. The potential and performance of the system was tested, and two- and three-dimensional imaging of different objects like human skin, infrared detection card, leaf, etc. has been presented.

Keywords: Biomedical imaging, optical coherence tomography, medical optics instrumentation, stratified media, swept-source laser.

BIOMEDICAL imaging using low coherence interferometer (LCI) with coherence gating, namely optical coherence tomography (OCT) was first demonstrated in 1991 by Haung *et al.*[1]. It is capable of generating noninvasive, noncontact, cross-sectional images of biological samples. Table 1 presents a comparison between OCT and other imaging techniques.

Some applications demand higher resolution with modest penetration in tissue. Confocal microscopy has the highest resolution with limited penetration depth. Thus, it is difficult to image deeper portions of biological samples. On the other hand, ultrasonography has excellent penetration in tissue, but lacks resolution. OCT fills the gap between confocal microscopy and ultrasonography. It utilizes low coherence interference and confocal gating to filter the light coming from different layers of an object. By changing the numerical aperture of scanning lenses, one can convert OCT to optical coherence microscopy (OCM). Resolution of OCM is high, but with compromise in its imaging depth.

OCT is mainly categorized into two types based on operating and detection mechanisms. First-generation OCT technology, namely time-domain OCT (TD-OCT) enabled scientists to generate relatively low resolution cross-sectional images of biological samples[1]. These low-quality images were due to poor sensitivity, slow imaging speed (caused by time consumption of scanning reference mirror) and mechanical instability of reference arm[1]. In TD-OCT, back and forth movement of reference mirror makes it hard to implement *in vivo* imaging of human eye in real time[1]. In order to improve imaging speed, sensitivity and signal-to-noise ratio (SNR), the second-generation OCT, namely Fourier-domain OCT (FD-OCT) was introduced[2]. In FD-OCT, two techniques are popular for *in vivo* imaging, namely spectral domain OCT (SD-OCT) and swept-source OCT (SS-OCT). There are other variations of OCT, like single-point OCT[3] and parallel or full-field OCT[4]. However, they are less popular in the *in vivo* clinical imaging.

SD-OCT has advantages over TD-OCT in terms of imaging speed, mechanical stability of the system due to fixed reference arm and increased sensitivity. It has been successfully implemented in *in vivo* imaging of various tissues. However, it has some limitations. SD-OCT is more suitable for 830 nm central wavelength than 1300 and 1060 nm wavelengths, which are appropriate for deeper penetration. At these two wavelengths, spectrometers, gratings and detectors are expensive and not compatible. Also, high-speed detectors or line cameras (CCD) are not available for these two wavelengths. Interference fringe washout is also a problem in SD-OCT while integrating signals with CCD/CMOS detectors[5]. Dual balanced detection is also difficult to implement with SD-OCT.

To overcome the above-mentioned problems, a high-speed, high-resolution, mechanically stable, noninvasive and noncontact OCT imaging system with tunable laser has been developed, namely SS-OCT[6]. Here, a broadband light source which consists of a spectrum of wavelengths dispatches one wavelength at a time (sweeping of wavelength) into the system. The backscattered light from the sample arm will interfere with a static reference arm and is detected by a single photodetector with respect to time of sweep, later scaled into wavenumber space using the k-clock signal[7–10]. After processing the signals, an inverse Fourier transform yields depth information of the sample[11]. The imaging speed is enhanced several times (~MHz) with SS-OCT, which is useful for *in vivo* imaging. A SS-OCT can also be used for a larger dynamic range; in such cases, dual balanced detection scheme is essential to achieve the shot noise-limited detection[10].

Figure 1 shows a typical SS-OCT set-up. Details of OCT theory are given elsewhere[12,13]. However, a brief description is given here. The reflected electrical fields at the beam splitter from reflected reference mirror and samples layers are

$$E_R = \frac{E_i}{\sqrt{2}} r_R \mathrm{e}^{i2kz_R}$$

and

$$E_S = \frac{E_i}{\sqrt{2}} \sum_{n-1}^{N} r_{S_n} \mathrm{e}^{i2kz_{S_n}}$$

*For correspondence. (e-mail: rpoddar@bitmesra.ac.in)

Table 1. Comparisons between optical coherence tomography (OCT) and other imaging techniques

Imaging modality	Resolution	Penetration depth in tissue	Contact or non-contact mode
Confocal microscopy	1 µm	Few 100 µm	Contact
Ultrasound imaging	Few 100 µm	Few centimetres	Contact
Computed tomography	Few 150 µm	Few 10 cm	Contact
Magnetic resonance imaging	1 to few mm	Few 100 cm	Contact
OCT	1–10 µm	Few millimetres	Non-contact

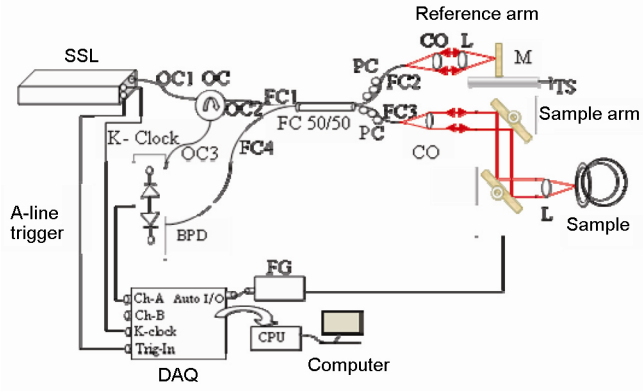

Figure 1. Schematic diagram of swept source optical coherence tomography (SS-OCT) system. SSL, Swept source laser; OC, Optical circulator; OC1, OC2, OC3, Optical circulator ports 1–3 respectively; FC 50/50, Fibre coupler 50/50; FC1, FC2, FC3, FC4, Fibre coupler ports 1–4 respectively; PC, Polarization controllers; CO, Collimator; L, Lens, M, Mirror; TS, Translation stage; BPD, Balanced photodetector; DAQ, Data acquisition board; FG, Function generator.

respectively. These two fields will interfere and produce an interference signal. The photocurrent (OCT) signal detected by the detector can be expressed as

$$I_D(k,\omega) = \frac{\rho}{2}\left\langle \left| \frac{H(k,\omega)}{\sqrt{2}} r_R e^{i(2kz_r - \omega t)} + \frac{H(k,\omega)}{\sqrt{2}} \sum_{n=1}^{N} r_{S_n} e^{i(2kz_{s_n} - \omega t)} \right|^2 \right\rangle.$$

Here, $E_i = H(k, \omega)e^{i(kz-\omega t)}$ is the incident electrical field on the reference mirror and sample (where $s(k, \omega)$ is the amplitude of broadband source spectrum, $k(=(2\pi/\lambda))$ the wavenumber, $\omega(=(2\pi/\lambda))$ the angular wavelength and $e^{i(kz-\omega t)}$ represents plane wave profile), r_R the reflectivity of the reference mirror, z_R the distance from beam splitter to the reference mirror, r_{S_n} the reflectivity from the nth sample layer, Z_{S_n} the distance from the beam splitter to the nth sample layer[13] and ρ is the responsivity of the detector. After simplification of the above equation, final time invariant OCT equation is given by[13]

$$I_D(k) = \frac{\rho}{2}\left[H(k)\left(R_r + \sum_{n=1}^{N} R_{S_n} \right) \right]$$

$$+ \frac{\rho}{4}\left[H(k)\sum_{n=1}^{N} \sqrt{R_r R_{S_n}} \left(e^{i2k(z_R - z_{S_n})} + e^{-i2k(z_R - z_{S_n})} \right) \right]$$

$$+ \frac{\rho}{4}\left[H(k) \sum_{n \neq m=1}^{N} \sqrt{R_{S_n} R_{S_m}} \left(e^{i2k(z_{S_n} - z_{S_m})} + e^{-i2k(z_{S_n} - z_{S_m})} \right) \right]. \quad (1)$$

Here $I_D(k)$ is the intensity of the OCT spectrum, $H(k)$ the spectrally encoded source spectrum of the light source or transfer function, R_r the reflectivity from the mirror and $\sum_{n-1}^{N} R_{S_n}$ is the reflectivity from different layers of the sample.

The proposed system has been developed based on the Michelson interferometer principle.

Light from a swept source laser (Axsun Technologies, USA, with central wavelength of 1064 nm, bandwidth of 110 nm and sweeping speed of 100 kHz) is fed into the fibre-based Michelson interferometer. It travels into the first port of the optical circulator (OC1) and emerges out from the second port (OC2). The emerged light travels into the 50–50 coupler, which splits the light intensity into 50 : 50 ratio – 50% of the input light goes into the reference arm and another 50% is directed to the sample arm. The reference arm comprises a collimator (focal length: 11.2 mm) and an achromatic doublet lens (focal length: 30 mm) used for focusing collimated beam onto a mirror which is mounted on a Z-axis translation stage. The sample arm comprises a collimator (focal length: 11.2 mm), X–Y axis Galvo scanner (Cambridge Technologies) and an achromataic doublet lens (focal length: 30 mm). In the sample arm, collimated beam incidents on galvo-scanner. Galvo-scanner receives the control signal from a function generator (model number: PCIe6363, National Instruments) in a synchronized manner with A-line trigger of the light source. Transverse resolution of the SS-OCT system depends on focal length and diameter of the focusing lens. In our system, transverse resolution is ~14 µm while axial resolution is ~5 µm. The reflected light from the sample and reference arm produces an interference signal at the 50–50 coupler. Fifty per cent of this light emerges from port 4, which is fed into one of the two input connectors of the balance photodetector (BPD). The remaining light emerges from port 1 of the 50–50 coupler and goes to an optical circulator. Further, light from port 3 is diverted into another input of BPD.

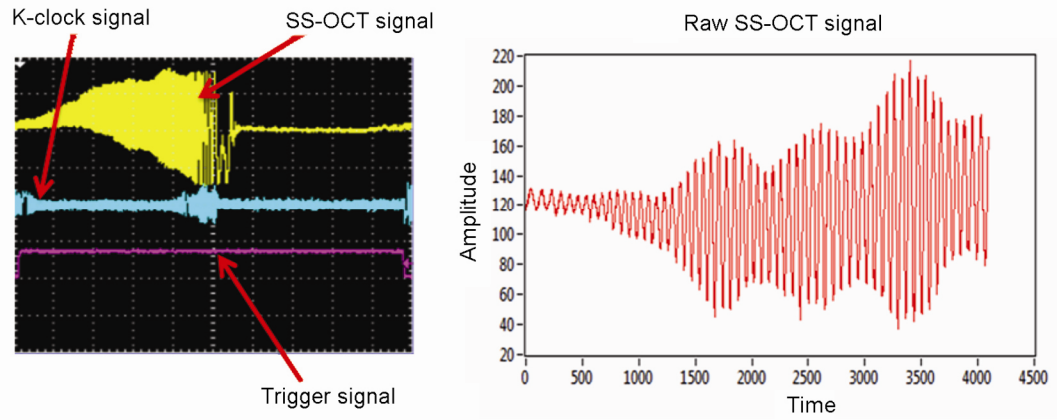

Figure 2. SS-OCT, k-clock and trigger signal captured with the mirror as sample with a digital oscilloscope.

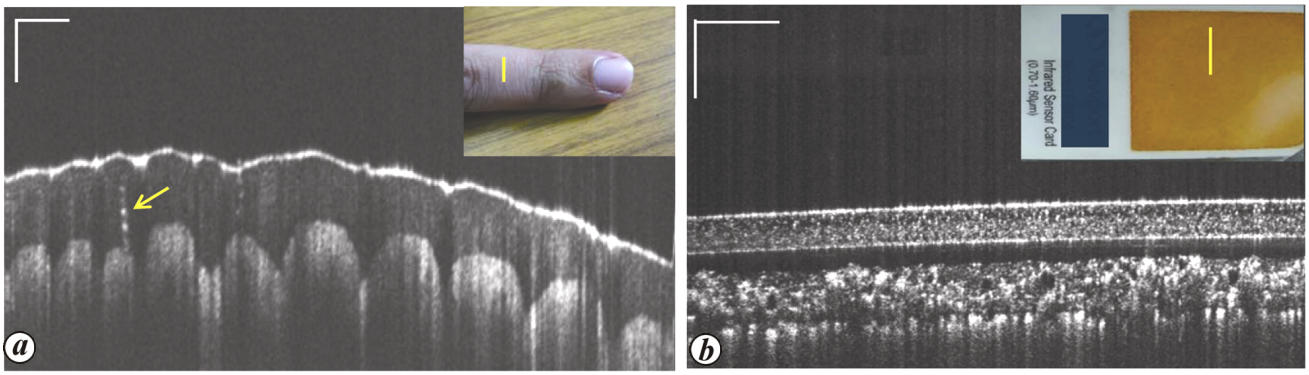

Figure 3. ***a***, OCT image of human skin (inset finger) acquired over 2.5 mm. Average intensity of ten B-scans from one position is shown. Yellow line indicates position of scanning area. Yellow arrow shows sebaceous gland. ***b***, OCT image of infrared (IR) detection card detector (inset IR card) acquired over 3.5 mm. Average intensity of ten B-scans from one position is shown. Scale bar: 500 µm.

Here, the optical circulator acts as an isolator, which prevents the back-reflected light from damaging the swept source.

The output from the detector is connected to Channel-A of a high-speed data acquisition board (ATS 9350, Alazar Technologies Inc, Canada). The clock input port of Data Acquisition Card (DAQ) is connected with the output k-clock signal from the swept source laser. The trigger input port of DAQ is attached to the trigger signal from the swept source laser. This trigger signal is used as a commanding reference signal for acquiring A-scan data length. The acquired signal is stored on a computer for post-processing of the signals.

After optimal alignment, the desired samples can be mounted on a sample holder at the end of sample arm. Scanning and data acquisition are controlled by a custom-made program. After obtaining the primary SS-OCT signal, polarization controllers are used to control the polarization state of the signal from reference and sample arms.

The SS-OCT signal is processed using standard post-processing method with a custom-made automated post-processing program, described in our earlier work[14]. In this program, the first step is removal of fixed pattern noise from the SS-OCT signal. De-noised SS-OCT signal is linear in wavenumber (k). Optical dispersion is numerically compensated using an automatic dispersion compensation based on entropy minimization method. Dispersion compensated signal is zero-padded. Finally, fast Fourier transform (FFT) is applied on the OCT signal to get B-scans.

Figure 2 represents a typical SS-OCT signal collected with mirror (single layer) in the sample arm, a k-clock signal and line-trigger captured with a digital oscilloscope (DSO). The SS-OCT signal is normally known as A-line profile. The k-clock signal from source is used for rescaling in wavenumber domain of OCT signal. Further, trigger signal is used for capturing the data.

Different stratified media namely, human skin from finger, infrared (IR) detection card (IR card) and leaf were imaged with the developed SS-OCT system. Figure 3 *a* shows the averaged B-scan OCT image of human skin. Different layers of the skin and sebaceous gland are clearly visible. The various layers of IR composite card,

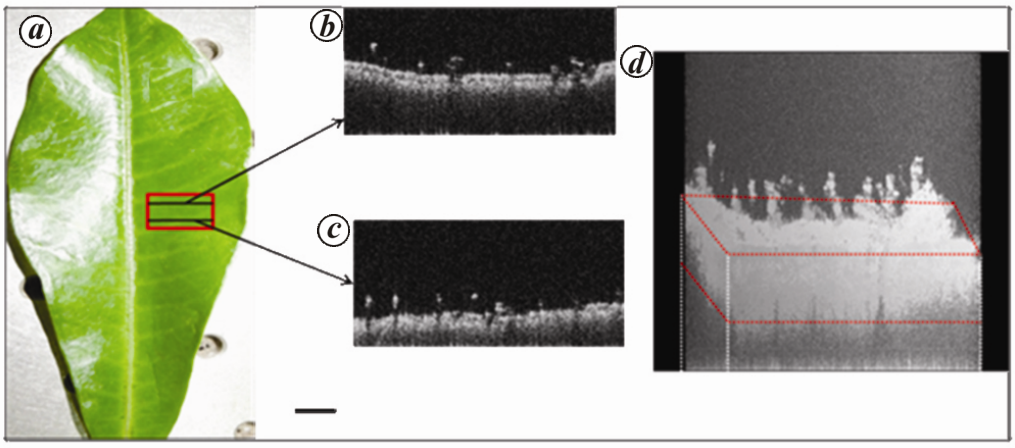

Figure 4. ***a***, Photograph of the leaf. ***b***, ***c***, B-scans of the leaf at the places marked places in (***a***); the B-scans were generated with 512 (A-lines) × 1024 (pixels) data points. ***d***, 3D volume image of the selected portion of the leaf generated with 512 (A-lines) × 1024 (pixels) × 65 (B-scans) data.

namely top plastic layer, fluorescent material layer and lower paper layer are also clearly visible (Figure 3 *b*).

The SS-OCT system is also capable of producing three-dimensional images of an object. A leaf was imaged with the system. Figure 4 *a* and *b* shows B-scans of the leaf from two different positions. Figure 4 *d* shows the 3D tomogram of the leaf.

Here, we have presented a high-speed, 1 μm SS-OCT system for *in vivo*, non-contact and noninvasive three-dimensional depth-resolved visualization different stratified media. The SS-OCT system provides detailed insights into cross-sectional images comparable to optical microcopy. SS-OCT is also capable of generating 3D images of any of the structures and media. Our data from different samples suggest that SS-OCT has potential in the detection of relative distances between different layers and their abnormalities for better understanding of pathogenesis, and studies of manufacturing faults in any composite material.

1. Huang, D. *et al.*, Optical coherence tomography. *Science*, 1991, **254**, 1178–1181.
2. Morgner, U., Drexler, W., Kärtner, F. X., Li, X. D., Pitris, C., Ippen, E. P. and Fujimoto, J. G., Spectroscopic optical coherence tomography. *Opt. Lett*., 2000, **25**, 111–113.
3. Fercher, A. F., Hitzenberger, C. K., Kamp, G. and El-Zaiat, S. Y., Measurement of intraocular distances by backscattering spectral interferometry. *Opt. Commun*., 1995, **117**, 43–48.
4. Anna, T., Srivastava, V., Shakher, C. and Mehta, D. S., Transmission mode full-field swept-source optical coherence tomography for simultaneous amplitude and quantitative phase imaging of transparent objects. *IEEE Photonics Technol. Lett*., 2011, **23**, 899–901.
5. Oldenburg, A., Xu, C. and Boppart, S., Spectroscopic optical coherence tomography and microscopy. *IEEE J. Sel. Top. Quantum Electron*., 2007, **13**, 1629–1640.
6. Wojtkowski, M., High-speed optical coherence tomography: basics and applications. *Appl. Opt*., 2010, **49**, 30–61.
7. De Boer, J. F., Barry, C., Park, B. H., Pierce, M. C., Tearney, G. J. and Bouma, B. E., Improved signal-to-noise ratio in spectral-domain compared with time-domain optical coherence tomography. *Opt. Lett.*, 2003, **28**, 2067–2069.
8. Wojtkowski, M., Leitgeb, R., Kowalczyk, A., Bajraszewski, T. and Fercher, A. F., *In vivo* human retinal imaging by Fourier domain optical coherence tomography. *J. Biomed. Opt*., 2002, **7**, 457–463.
9. Potsaid, B. *et al.*, Ultrahigh speed 1050 nm swept source/Fourier domain OCT retinal and anterior segment imaging at 100,000 to 400,000 axial scans per second. *Opt. Express*, 2010, **18**, 20029–20048.
10. Yun, S. H., Tearney, G., De Boer, J. F., Iftimia, N. and Bouma, B., High-speed optical frequency-domain imaging. *Opt. Express*, 2003, **11**, 2953–2963.
11. Braaf, B., Vermeer, K. A., Sicam, V. A. D. P., van Zeeburg, E., van Meurs, J. C. and De Boer, J. F., Phase-stabilized optical frequency domain imaging at 1-μm for the measurement of blood flow in the human choroid. *Opt. Express*, 2011, **19**, 20886–20903.
12. Lim, H., Mujat, M., Kerbage, C., Lee, E. C., Chen, Y., Chen, T. C. and De Boer, J. F., High-speed imaging of human retina *in vivo* with swept-source optical coherence tomography. *Opt. Express*, 2006, **14**, 12902–12908.
13. Izatt, J. A. and Choma, M. A., *Theory of Optical Coherence Tomography*, Springer, Berlin, 2008, pp. 47–72.
14. Poddar, R. and Reddikumar, M., *In vitro* 3D anterior segment imaging in lamb eye with extended depth range swept source optical coherence tomography. *Opt. Laser Technol*., 2015, **67**, 33–37.

ACKNOWLEDGEMENTS. We thank the Department of Science and Technology, Government of India for financial support (IDP/MED/10/2010). M.R. thanks BIT-Mesra, Ranchi for scholarship.

Received 15 September 2015; revised accepted 24 August 2017

doi: 10.18520/cs/v114/i02/374-377